Available online at www.sciencedirect.com
ScienceDirect
Ceramics International 34 (2008) 1533–1537
CERAMICS INTERNATIONAL
www.elsevier.com/locate/ceramint

Precursor effects on ZrW_2O_8 formation kinetics

Jun-ichi Tani *, Hiroyasu Kido

Department of Electronic Materials, Osaka Municipal Technical Research Institute, 1-6-50 Morinomiya, Joto-ku, Osaka 536-8553, Japan

Received 22 January 2007; received in revised form 31 March 2007; accepted 25 April 2007
Available online 2 June 2007

Abstract

The synthesis of ZrW_2O_8 from different kinds of mixtures containing ZrO_2–WO_3, $ZrO(NO_3)_2{\cdot}2H_2O$–WO_3, $ZrCl_2O{\cdot}8H_2O$–WO_3, and ZrO_2–$(NH_4)_{10}W_{12}O_{41}{\cdot}5H_2O$ was investigated, and the kinetics was analyzed using JMA equation. It was found that $ZrO(NO_3)_2{\cdot}2H_2O$, $ZrCl_2O{\cdot}8H_2O$ H_2O and $(NH_4)_{10}W_{12}O_{41}{\cdot}5H_2O$ that were used as inorganic precursors formed ZrO_2 and WO_3 after firing above 500 °C. The content of ZrW_2O_8 obtained by firing the mixtures is influenced by the kinds of precursors as well as mixing methods. The formation rate of ZrW_2O_8 depends on homogeneity related to mixing methods as well as the particle size of starting powders. Phase-pure ZrW_2O_8 is obtained from the $ZrCl_2O{\cdot}8H_2O$–WO_3 mixtures at 1200 °C for 4 h, which is much shorter time than in the case of conventional ZrO_2–WO_3 mixtures. In the reaction kinetics of ZrO_2–WO_3 system, the Avrami exponent (n) is ~0.5 above 1175 °C, indicating that the reaction is controlled by the diffusion-controlled reaction.

Keywords: A. Powders: solid state reaction; B. X-ray methods; E. Thermal applications; ZrW_2O_8

1. Introduction

Zirconium tungstate, ZrW_2O_8, was shown to exhibit isotropic negative thermal expansion over a wide temperature range from 0.3 to 1050 K [1,2]. The traditional way of preparing ZrW_2O_8 is a solid-state reaction route of zirconium oxide and tungsten oxide at 1200 °C for 12–72 h [3–6]. However, it takes a long time in order to obtain pure phase ZrW_2O_8 and the high temperatures used for the solid state reaction lead to tungsten oxide volatilization. For this reason, alternative methods have been proposed to synthesize ZrW_2O_8 that would allow for lower synthesis temperature. The methods are based on chemical synthesis routes such as sol–gel method [7] and hydrothermal synthesis method [8].

There are few reports concerning the influence of zirconium precursors as well as tungsten precursors on the formation of ZrW_2O_8. Microencapsulation is a process whereby a core material is occluded by a coating of another phase and is advantageous for controlling the scale of segregation and distribution of components and for reducing diffusion distances between components [9]. However, there are no reports concerning the synthesis of ZrW_2O_8 using microencapsulation method of inorganic precursors in order to increase the solid-state reactivity. Moreover, the reaction mechanism of ZrW_2O_8 formation has not been investigated.

In the present study, we report the formation of ZrW_2O_8 by firing four different kinds of mixtures, namely, ZrO_2–WO_3, zirconium oxynitrate dihydrate ($ZrO(NO_3)_2{\cdot}2H_2O$)–WO_3, zirconium oxychloride octahydrate ($ZrCl_2O{\cdot}8H_2O$)–WO_3, and ZrO_2–ammonium tungstate *para* pentahydrate ($(NH_4)_{10}W_{12}O_{41}{\cdot}5H_2O$). The effects of the kinds of starting materials on the formation of ZrW_2O_8 and the mechanism of ZrW_2O_8 formation are discussed.

2. Experimental procedures

Fig. 1 shows a process flow chart for preparing fired pellets. Commercially available high-purity zirconium oxide (ZrO_2; Nakarai Tesque, Kyoto, Japan), tungsten oxide (WO_3; Nakarai Tesque), zirconium oxynitrate dihydrate ($ZrO(NO_3)_2{\cdot}2H_2O$; Wako Pure Chemical Industries, Osaka, Japan), zirconium oxychloride octahydrate ($ZrCl_2O{\cdot}8H_2O$; Wako Pure Chemical Industries), ammonium tungstate *para* pentahydrate ($(NH_4)_{10}W_{12}O_{41}{\cdot}5H_2O$; Wako Pure Chemical Industries) were used as starting materials in this study. In ZrO_2–WO_3 system, stoichiometric mixtures of the stating

* Corresponding author. Tel.: +81 6 6963 8081; fax: +81 6 6963 8099.
E-mail address: tani@omtri.city.osaka.jp (J.-i. Tani).

0272-8842/$34.00
doi:10.1016/j.ceramint.2007.04.015

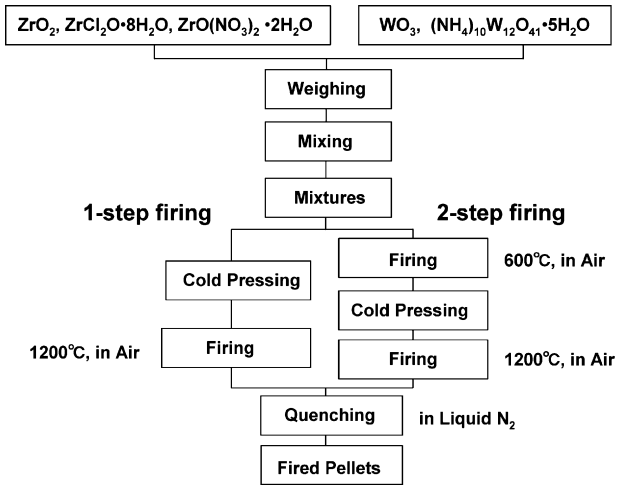

Fig. 1. Process flow chart for preparing fired pellets.

powders were prepared using dry ball-milling or wet ball-milling in ethanol with polyethlyethylene jar in zirconia media for 10 min–24 h. For inorganic precursor microencapsulated systems ($ZrO(NO_3)_2{\cdot}2H_2O$–WO_3, $ZrCl_2O{\cdot}8H_2O$–WO_3 and ZrO_2–$(NH_4)_{10}W_{12}O_{41}{\cdot}5H_2O$), the mixtures were produced by stirring in water. The mixtures (0.05 M) were aged in a water bath with stirring by a magnetic stirrer at 100 °C for 5 h and then dried.

1.5 g powder mixtures were pressed at 60 MPa into pellets (13 mm in diameter) using a hand press, and fired in air to 1200 °C with a dwell time of 5 min–8 h in a Pt crucible. The heating rate was 20 °C/min. The heated pettets were then rapidly quenched in liquid nitrogen. For the inorganic precursor microencapsulated systems, a two-step firing process was investigated. In two-step firing process, a separate burnout step was done at 600 °C for 3 h before pressing and firing to eliminate a large volume of volatile species because of the high weight loss associated with inorganic precursor decomposition prior to solid state reaction.

A scanning electron microscope (model JSM-6460LA, JEOL, Tokyo, Japan) was used at 20 kV with a working distance 20 mm to characterize the starting powder and the mixtures. Particle sizes of starting powders were determined by laser diffraction and scattering method (model LA-920, Horiba Ltd., Kyoto, Japan). Specific surface areas of starting powders were measured using the Brunauer–Emmerr–Teller (BET) method utilizing absorption nitrogen gas at −196 °C. Prior to measurement, the powders were outgassed at 150 °C for 3 h.

Phase analysis was performed with X-ray powder diffraction (XRD; model RINT 2500, Rigaku, Tokyo) which utilized Cu Kα radiation at 40 kV and 50 mA. Phase identification was accomplished by comparing the experimental XRD patterns to standards compiled by the International Center for Diffraction Data (ICDD). Quantitative analysis of fraction of ZrW_2O_8 present was done by matrix-flushing method by Chung [10]. α-Al_2O_3 was used as a flushing agent. The content of ZrW_2O_8 in each sample was determined by calculating the integrated peak intensities of ZrW_2O_8 and α-Al_2O_3 in XRD patterns.

3. Results and discussion

Fig. 2 shows scanning electron microscope (SEM) micrographs of commercially available monoclinic ZrO_2 (ICDD Card No. 88-2390) and monoclinic WO_3 (ICDD Card No. 72-1465) used in this study. The mean volume particle sizes of ZrO_2 and WO_3 determined by laser diffraction and scattering method are 5.5 and 0.2 μm, respectively. The specific surface areas (S_w) of ZrO_2 and WO_3 determined by the BET method are 8.6 and 4.2 m^2/g, respectively. The primary particle sizes of ZrO_2 and WO_3 estimated from the equation: $d_{BET} = 6/(\rho S_w)$, where ρ is density, are 0.13 and 0.20 μm, respectively. The mean volume particle size of WO_3 determined by laser diffraction and scattering method is in good agreement with the primary particle size estimated using the BET method.

Table 1 summarizes of TGA data of various precursors under flowing air at the flow rate of 300 ml/min with a heating rate of 10 °C/min. XRD analyses showed that products obtained by firing $ZrO(NO_3)_2{\cdot}2H_2O$, $ZrCl_2O{\cdot}8H_2O$ H_2O and $(NH_4)_{10}W_{12}O_{41}{\cdot}5H_2O$ above 600 °C show monoclinic ZrO_2 (ICDD Card No. 88-2390) and monoclinic WO_3 (ICDD Card No. 72-1465), respectively. For $ZrO(NO_3)_2{\cdot}2H_2O$ and $ZrCl_2O{\cdot}8H_2O$, the percentage of weight is 38.3 and 45.6% above 490 and 525 °C, respectively. These values are in good agreement with the weight ratios of ZrO_2/$ZrO(NO_3)_2{\cdot}2H_2O$ (38.2%) and ZrO_2/$ZrCl_2O{\cdot}8H_2O$ (46.1%). For

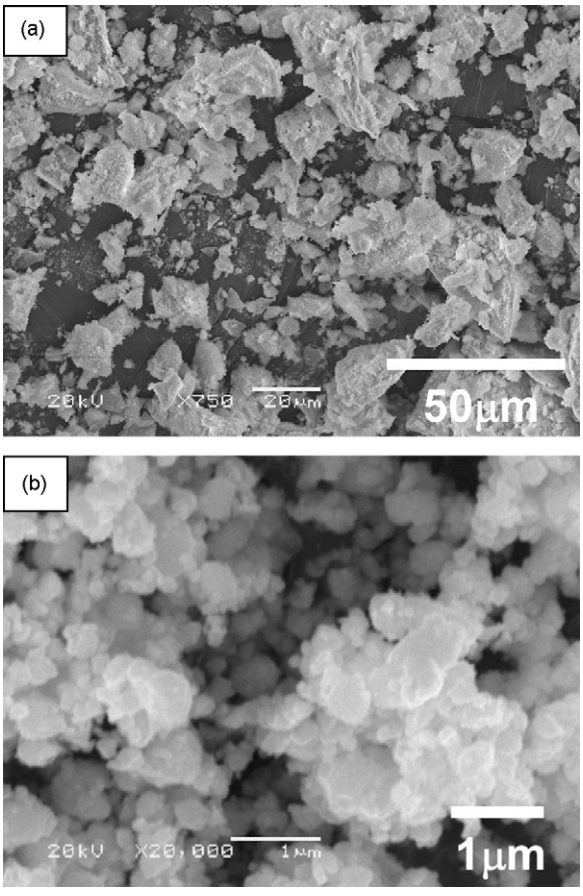

Fig. 2. SEM micrographs of starting powders (a) ZrO_2 and (b) WO_3.

Table 1
Results of TGA data of various precursors under flowing air at the flow rate of 300 ml/min with a heating rate of 10 °C/min

Precursors	Temperature (°C)[a]	Weight (%)[b]	Weight (calculation) (%)[c]
Zirconium oxynitrate dihydrate	490	38.3	38.2
Zirconium oxychloride octahydrate	525	45.6	46.1
Ammonium tungstate *para* pentahydrate	450	89.3	88.8

[a] The temperature above which there is no further weight loss.
[b] Weight percentage measured by TGA.
[c] Weight percentage calculated by the chemical formula.

$(NH_4)_{10}W_{12}O_{41}\cdot 5H_2O$, the percentage of weight (89.3%) above 450 °C is in good agreement with the weight ratio of $WO_3/(NH_4)_{10}W_{12}O_{41}\cdot 5H_2O$ (88.8%).

Fig. 3 shows XRD results of the products obtained by firing ZrO_2–WO_3 at 1200 °C for 15 min using two mixing methods, namely dry milling for 10 min and wet milling for 24 h. α-ZrW_2O_8 phase (ICDD Card No. 87-1528) was detected in the products obtained by firing ZrO_2–WO_3 at 1200 °C and the content of ZrW_2O_8 in the products is 62.1 and 91.1 wt%, respectively. This result shows that the amount of ZrW_2O_8 is drastically affected by mixedness of the mixture of ZrO_2 and WO_3. The color of the products obtained by firing ZrO_2–WO_3 at 1200 °C for 24 h is yellowish and suggests that a small amount of yellow WO_3 exist in the products. In fact, very weak XRD peaks of WO_3 were found to exist in the products obtained by firing ZrO_2–WO_3 at 1200 °C for 24 h. Therefore, it is difficult to obtain phase pure ZrW_2O_8 from conventional mixture of ZrO_2 and WO_3 in a short time.

Fig. 4 shows XRD results of the products obtained by firing ZrO_2–WO_3, $ZrO(NO_3)_2\cdot 2H_2O$–WO_3, $ZrCl_2O\cdot 8H_2O$–WO_3 and ZrO_2–$(NH_4)_{10}W_{12}O_{41}\cdot 5H_2O$ at 1200 °C for 5 min. For inorganic precursor microencapsulated systems: $ZrO(NO_3)_2\cdot 2H_2O$–WO_3, $ZrCl_2O\cdot 8H_2O$–WO_3 and ZrO_2–$(NH_4)_{10}W_{12}O_{41}\cdot 5H_2O$, the mixtures were produced by stirring in water. $ZrCl_2O\cdot 8H_2O$, $ZrO(NO_3)_2\cdot 2H_2O$–WO_3 and $(NH_4)_{10}W_{12}O_{41}\cdot 5H_2O$ dissolved in water at room temperature and reprecipitated upon drying the mixtures. The mixture was evaporated to dryness on a hot plate, dried at 100 °C for 48 h in an oven and then fired at 600 °C. The height of XRD peaks of ZrO_2 and WO_3 obtained by firing inorganic precursors; $ZrO(NO_3)_2\cdot 2H_2O$, $ZrCl_2O\cdot 8H_2O$ and

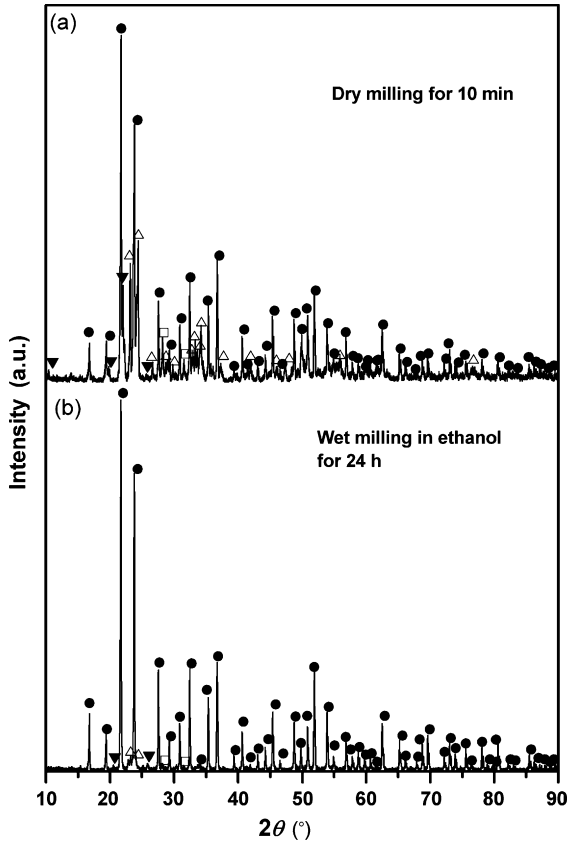

Fig. 3. XRD patterns of products obtained by firing ZrO_2–WO_3 at 1200 °C for 15 min using two mixing methods: (a) dry milling for 10 min; (b) wet milling in ethanol for 24 h [(●) ZrW_2O_8, (△) WO_3, (□) ZrO_2, (▼) unknown phase].

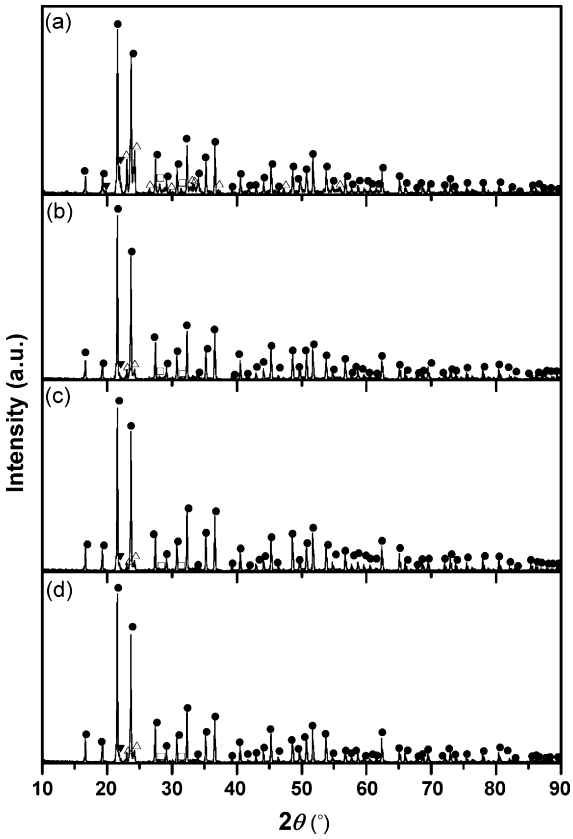

Fig. 4. XRD patterns of products obtained by firing (a) ZrO_2–WO_3, (b) $ZrO(NO_3)_2\cdot 2H_2O$–WO_3, (c) $ZrCl_2O\cdot 8H_2O$–WO_3 and (d) ZrO_2–$(NH_4)_{10}W_{12}O_{41}\cdot 5H_2O$ at 1200 °C for 5 min [(●) ZrW_2O_8, (△) WO_3, (□) ZrO_2, (▼) unknown phase].

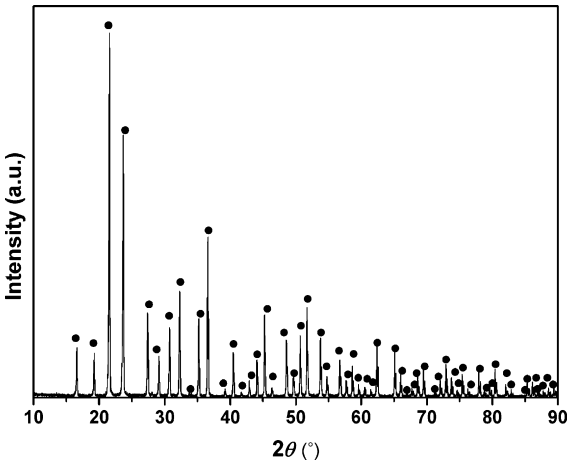

Fig. 5. XRD patterns of products obtained by firing $ZrCl_2O{\cdot}8H_2O$–WO_3 at 1200 °C for 4 h [(●) ZrW_2O_8].

$(NH_4)_{10}W_{12}O_{41}{\cdot}5H_2O$ at 600 °C is lower than that of commercially available starting powders of ZrO_2 and WO_3 used in this study. The lower XRD peaks will reflect smaller particle sizes of ZrO_2 and WO_3. The content of ZrW_2O_8 in the products by firing wet ball-milled ZrO_2–WO_3, $ZrO(NO_3)_2{\cdot}2H_2O$–WO_3, $ZrCl_2O{\cdot}8H_2O$–WO_3 and ZrO_2–$(NH_4)_{10}W_{12}O_{41}{\cdot}5H_2O$ at 1200 °C at the dwell time of 5 min is 72.4, 89.7, 93.0 and 91.3 wt%, respectively. The amount of ZrW_2O_8 by firing $ZrO(NO_3)_2{\cdot}2H_2O$–WO_3, $ZrCl_2O{\cdot}8H_2O$–WO_3 and ZrO_2–$(NH_4)_{10}W_{12}O_{41}{\cdot}5H_2O$ is larger than that by firing wet ball-milled ZrO_2–WO_3. This result indicates that the formation rate of ZrW_2O_8 from the inorganic precursor microencapsulated systems is faster than conventional ZrO_2–WO_3 mixtures. As discussed above, it takes a long time in order to obtain phase-pure ZrW_2O_8 by firing conventional ZrO_2–WO_3 mixtures. In our experiment, a very small amount of WO_3 is still left in the products by firing wet ball-milled ZrO_2–WO_3 at 1200 °C for 24 h. However, as shown in Fig. 5, phase-pure white ZrW_2O_8 is obtained by firing $ZrCl_2O{\cdot}8H_2O$–WO_3 in the product obtained by reacting at 1200 °C at the dwell time of 4 h, which is much shorter time than from conventional ZrO_2–WO_3 mixtures.

To clarify the reaction kinetics of ZrW_2O_8 formation, the solid state reaction kinetics of ZrO_2–WO_3 mixtures was examined. Hancock and Sharp [11] proposed the application of the generalized Avrami formula [12–14] for comparing the solid-state kinetics data. In general, the Johnson–Mehl–Avrami (JMA) kinetics equation is given by:

$$y = 1 - \exp[-(kt)^n], \tag{1}$$

where y is the fraction of the phase formed at a given temperature in time t, k the reaction rate constant, and n the Avrami exponent.

k is related to the activation energy of the process, E_a, through the Arrhenius temperature dependence,

$$k = A\exp\left(-\frac{E_a}{RT}\right), \tag{2}$$

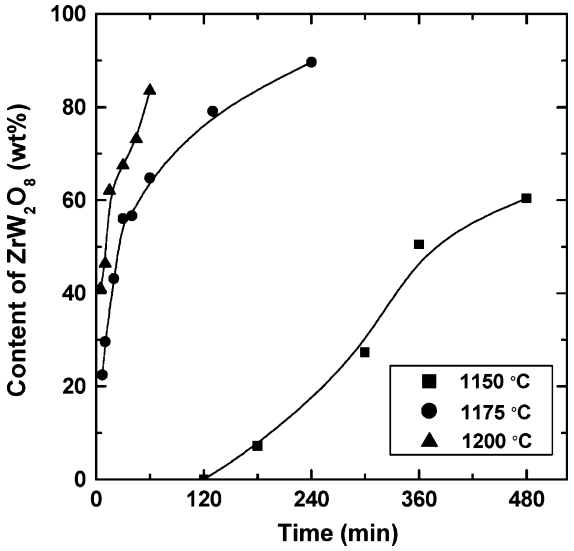

Fig. 6. Content of ZrW_2O_8 as a function of reaction time at various temperatures for ZrO_2–WO_3 system. The ZrO_2–WO_3 mixtures were prepared using dry ball-milling for 10 min. Heating rate is 20 °C/min.

The logarithm followed by a rearrangement of Eq. (1) yields

$$\ln\left[\ln\left(\frac{1}{1-y}\right)\right] = n\ln k + n\ln t, \tag{3}$$

Fig. 6 shows the weight percentages of ZrW_2O_8 phase obtained from a dry ball-milled ZrO_2–WO_3 mixture for 10 min as a function of reaction time. The following reaction between ZrO_2 and WO_3 starts above 1150 °C.

$$ZrO_2(s) + 2WO_3(s) \rightarrow ZrW_2O_8(s), \tag{4}$$

The phase content of ZrW_2O_8 increases with increasing reaction time and temperature. The content of ZrW_2O_8 in the products obtained by reacting at 1175 and 1200 °C at the dwell time of 1h is 64.8 and 83.5 wt%, respectively. At 1150 °C,

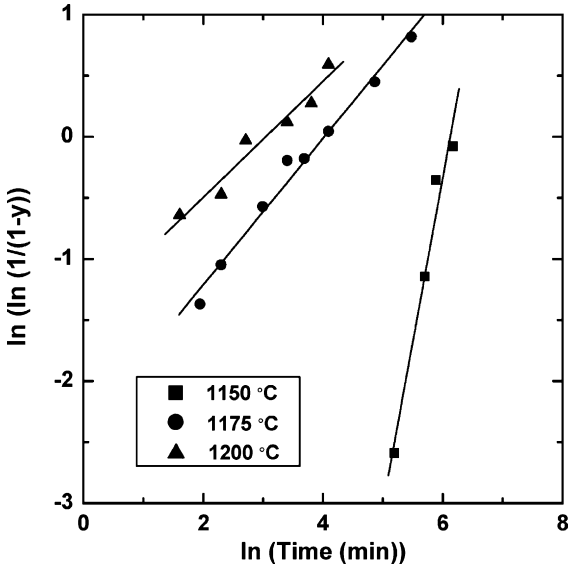

Fig. 7. Reaction kinetics fitted by the Johnson–Mehl–Avrami equation in ZrO_2–WO_3 system.

however, no ZrW_2O_8 exists in the products obtained by reacting ZrO_2–WO_3 at the beginning of reaction time, for example, 120 min. Fig. 7 shows the ln[ln (1/(1 − y))] versus ln(time) in ZrO_2–WO_3 system. The dependence of ln[ln(1/(1 − y))] on ln(time) gives a straight line in the whole investigated dwell time region. The values of n in case of reaction temperature of 1150, 1175 and 1200 °C are 2.7, 0.6 and 0.47, respectively. The activation energy E_a is determined to be 696 kJ/mol from the slope of ln (k) − 1/T plots. A value close to 0.5 above 1175 °C indicates that the rate-controlling step is a diffusion mechanism [11]. Therefore, it is important to reduce the scale of segregation and diffusion distances between components by controlling mixedness as well as using a small particle size of starting powders in order to synthesis phase-pure ZrW_2O_8.

4. Conclusions

The synthesis of ZrW_2O_8 from different kinds of mixtures containing ZrO_2–WO_3, $ZrO(NO_3)_2{\cdot}2H_2O$–WO_3, $ZrCl_2O{\cdot}8H_2O$–WO_3, and ZrO_2–$(NH_4)_{10}W_{12}O_{41}{\cdot}5H_2O$ was investigated, and the kinetics was analyzed using JMA equation. It was found that $ZrO(NO_3)_2{\cdot}2H_2O$, $ZrCl_2O{\cdot}8H_2O$ H_2O and $(NH_4)_{10}W_{12}O_{41}{\cdot}5H_2O$ that were used as inorganic precursors formed ZrO_2 and WO_3 after firing above 500 °C. The content of ZrW_2O_8 obtained by firing the mixtures is influenced by the kinds of precursors as well as mixing methods. The formation rate of ZrW_2O_8 depends on homogeneity related to mixing methods as well as the particle size of starting powders. Phase-pure ZrW_2O_8 is obtained from the $ZrCl_2O{\cdot}8H_2O$–WO_3 mixtures at 1200 °C for 4 h, which is much shorter time than in the case of conventional ZrO_2–WO_3 mixtures. In the reaction kinetics of ZrO_2–WO_3 system, the Avrami exponent (n) is ∼0.5 above 1175 °C, indicating that the reaction is controlled by the diffusion-controlled reaction.

References

[1] T.A. Mary, J.S.O. Evans, T. Vogt, A.W. Sleight, Negative thermal expansion from 0.3 to 1050 Kelvin in ZrW_2O_8, Science 272 (1996) 90–92.

[2] J.S.O. Evans, T.A. Mary, T. Vogt, M.A. Subramanian, A.W. Sleight, Negative thermal expansion in ZrW_2O_8 and HfW_2O_8, Chem. Mater. 8 (1996) 2809–2823.

[3] U. Kameswari, A.W. Sleight, J.S.O. Evans, Rapid synthesis of ZrW_2O_8 and related phases, and structure refinement of $ZrWMoO_8$, Int. J. Inorg. Mater. 2 (2000) 333–337.

[4] Y. Morito, S. Wang, Y. Ohshima, T. Uehara, T. Hashimoto, Preparation of dense negative-thermal-expansion oxide by rapid quenching of ZrW_2O_8 melt, J. Ceram. Soc. Jpn. 110 (2002) 544–548.

[5] T. Hashimoto, T. Katsube, Y. Morito, Observation of two kinds of phase transitions of ZrW_2O_8 by power-compensated differential scanning calorimetry and high temperature X-ray diffraction, Solid State Commun. 116 (2000) 129–132.

[6] Y. Yamamura, N. Nakajima, T. Tsuji, Heat capacity anomaly due to the α-to-β structural phase transition in ZrW_2O_8, Solid State Commun. 114 (2000) 453–455.

[7] A.P. Wilkinson, C. Linda, S. Pattanaik, A new polymorph of ZrW_2O_8 prepared using nonhydrolytic sol–gel chemistry, Chem. Mater. 11 (1999) 101–108.

[8] C. Closmann, A.W. Sleight, Low-temperature synthesis of ZrW_2O_8 and Mo-substituted ZrW_2O_8, J. Solid. State. Chem. 139 (1998) 424–426.

[9] P.R. Mort, R.E. Riman, Reactive multicomponent powder mixtures prepared by microencapsulation: $Pb(Mg_{1/3}Nb_{2/3})O_3$ synthesis, J. Am. Ceram. Soc. 75 (1992) 1581–1586.

[10] F.H. Chung, Quantitative interpretation of X-ray diffraction patterns of mixtures. I. matrix-flushing method for quantitative multicomponent analysis, J. Appl. Cryst. 7 (1974) 519–525.

[11] J.D. Hancock, J.H. Sharp, Method of comparing solid-state kinetic data and its application to the decomposition of kaolinite, brucite, and $BaCO_3$, J. Am. Ceram. Soc. 55 (1972) 74–77.

[12] M. Avrami, Kinetics of phase change, I: general theory, J. Chem. Phys. 7 (1939) 1103–1112.

[13] M. Avrami, Kinetics of phase change, II: transformation-time relations for random distribution of nuclei, J. Chem. Phys. 8 (1940) 212–224.

[14] M. Avrami, Kinetics of phase change, III: granulation, phase change, and microstructure, J. Chem. Phys. 9 (1941) 177–187.